ACS OMEGA

http://pubs.acs.org/journal/acsodf

Article

Minimalistic Artificial Catalysts with Esterase-Like Activity from Multivalent Nanofibers Formed by the Self-Assembly of Dipeptides

Ning Liu, Shuai-Bing Li, Yan-Zhen Zheng, Su-Ying Xu, and Jiang-Shan Shen*

Cite This: *ACS Omega* 2023, 8, 2491−2500

Read Online

ACCESS | Metrics & More | Article Recommendations | Supporting Information

ABSTRACT: Imitating and incorporating the multiple key structural features observed in natural enzymes into a minimalistic molecule to develop an artificial catalyst with outstanding catalytic efficiency is an attractive topic for chemists. Herein, we designed and synthesized one class of minimalistic dipeptide molecules containing a terminal −SH group and a terminal His-Phe dipeptide head linked by a hydrophobic alkyl chain with different lengths, marked as HS-C_{n+1}-His-Phe (n = 4, 7, 11, 15, and 17; n + 1 represents the carbon atom number of the alkyl chain). The His (−imidazole), Phe ($-CO_2^-$) moieties, the terminal −SH group, and a long hydrophobic alkyl chain were found to have important contributions to achieve high binding ability leading to outstanding absolute catalytic efficiency (k_{cat}/K_M) toward the hydrolysis reactions of carboxylic ester substrates.

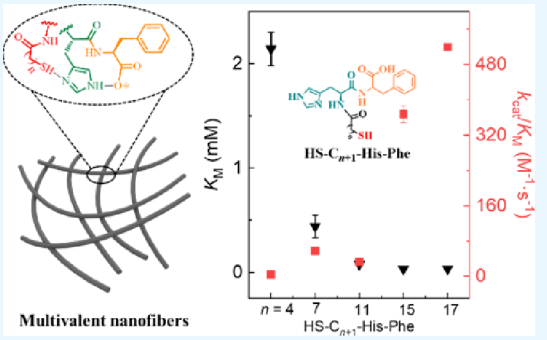

INTRODUCTION

It is well known that intricate chemical processes in living systems can be elegantly controlled by enzymes functioning as catalysts due to their powerful catalytic performance and extraordinary specificity.[1,2] In particular, hydrolase, as a vital and ubiquitous family of enzymes, can catalyze the breakdown reactions of a series of important chemical bonds including carboxylic ester, phosphate ester, and amide bonds which have received extensive attention in view of the importance of these chemical bonds for constituting biomolecules such as glycerides, nucleic acids, and proteins, respectively.[3−5] The unrivaled catalytic ability of natural hydrolases mainly stems from their unique ability to fold peptide chains into tertiary structures guided by several weak interactions such as hydrophobic, hydrogen bonding, and van der Waals force interactions.[6,7] This folding can lead to the fact that remote active-site residues can be brought into close proximity to create a hydrophobic pocket required for binding and catalysis for substrates in nature.[8]

Considerable efforts, to clarify the key structures and the active-site of natural hydrolases, have been made by biologists and chemists.[9,10] α-Chymotrypsin (α-ChS), a textbook example of the hydrolase structure, contains serine (Ser), histidine (His), and aspartate (Asp) residues, known as a catalytic triad which plays the roles of a nucleophile, a general base, and a hydrogen bonding acceptor, respectively, together with a hydrophobic domain, to constitute a hydrophobic pocket, to attract, partition, and align substrates (Figure 1a).[11] Besides the active-site and hydrophobic pocket, another important structural feature of these natural hydrolases is oxyanion holes, usually composed of amide functionalities. These oxyanion holes can stabilize reaction intermediates and transition states by forming hydrogen bonds to reduce the activation energy of the catalytic reactions.[12]

Therefore, how to imitate multiple key structural features to develop synthetic catalyst systems that show similar chemistry to natural hydrolases is a long-standing challenge for chemists. For example, Connal and co-workers ingeniously combined the active-site chemistry, hydrophobic environment, and oxyanion hole to develop an enzyme-inspired catalytic system.[13] This three-component micellar system is composed of co-surfactants cetyltrimethylammonium bromide, hexadecyl guanidinium hydrochloride, and ACT-C_{16} containing an imidazole, −OH, and −COOH in close proximity, with high catalytic activity for carboxylic ester hydrolysis. Not surprisingly, designing and developing these artificial hydrolase-like catalysts are attractive, considering that they can overcome some operational limitations of natural enzymes; for example, in general the activity of natural enzymes is easily disrupted by the changes of some experimental conditions.[14,15]

Nonetheless, the catalytic efficiencies of most of developed protease mimics are modest with respect to natural enzymes, which has been realized by scientists to mainly result from their low structural complexity.[16−18] Therefore, the multivalent scaffold-based protease mimics, such as early micelles/vesicles,[19,20] later dendrimers,[21,22] and metal nanopar-

Received: October 29, 2022
Accepted: December 21, 2022
Published: December 30, 2022

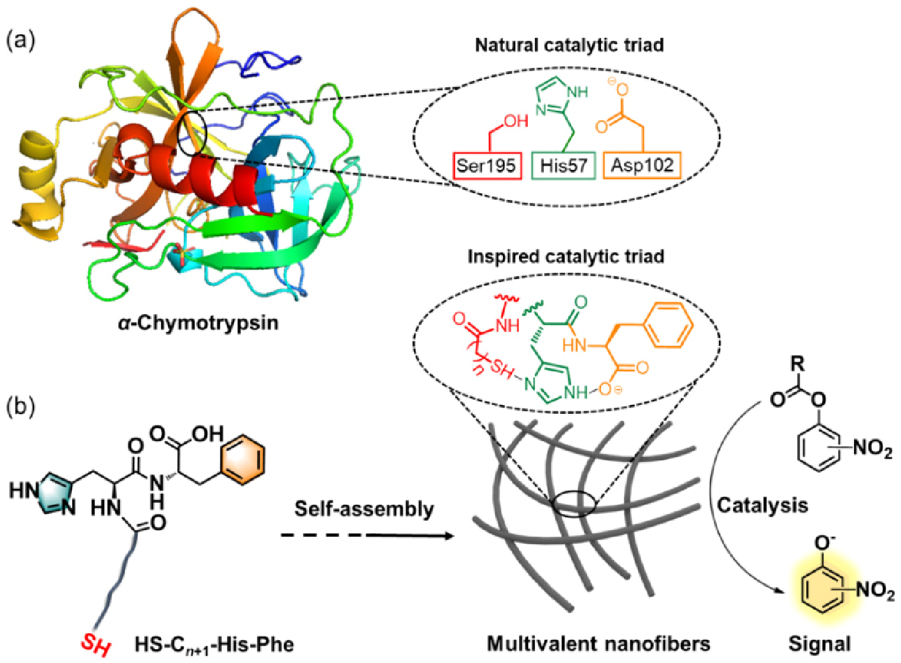

Figure 1. Crystal structure of natural α-chymotrypsin (a) and the schematic diagram of the hydrolysis reaction of a carboxylic ester catalyzed by the self-assembled multivalent nanofibers (HS-C$_{n+1}$-His-Phe) in this work (b).

ticles,[23−25] have been developed to be expected to increase structural complexity to obtain outstanding catalytic efficiencies. In particular, developing small self-assembled peptides to establish supramolecular catalysis is interesting, considering the aggregation driven by hydrophobic interaction and hydrogen bonding interaction in some alkylated peptides cases to self-assemble into micelles,[26] vesicles,[27] nanofibers,[28−30] and so on, and driven by the catalytic sites anchored on the surface of Au nanoparticles to generate multivalent systems, via Au−S bonds and electrostatic attractive interaction.[18,31] We should note that the latter monolayer-protected gold nanoparticles, first reported by Scrimin's group as a pioneering study,[23] exhibited high catalytic efficiencies in the cleavage reaction of 2-hydroxypropyl-4-nitrophenyl phosphate, an RNA-model compound, ascribed to their multivalent nature. Furthermore, a multivalent Ag−SR coordination polymer system bearing 1,4,7-triazacyclononane·Zn^{2+} (TACN·Zn^{2+}) complexes as catalytic heads was recently reported by us.[32] It was found that the self-assembled polymers possess extraordinary phosphatase-like catalytic activity toward the hydrolysis reaction of this phosphodiester.[32] Although the increment of structural complexity can show a significant contribution to access high catalytic activity, minimalistic molecules are expected to be created to achieve the goal in a very simple way to avoid complexing design and tedious synthesis yet these systems generally show modest activity.[33,34] This is a contradictory problem. Therefore, we asked whether or not by incorporating the above-mentioned several key structural elements into a single minimalistic molecule to readily self-assemble to create a multivalent structure driven by weak noncovalent interactions with an outstanding catalytic efficiency. If this can be achieved, it will bridge the gap between structural complexity and minimalist.

In this work, we designed and synthesized a series of minimalistic dipeptide molecules containing a terminal −SH group linked by hydrophobic alkyl chains of varying lengths. This dipeptide head containing a His residue and a phenylalanine (Phe) residue is expected to be close to the −SH group originating from the same or another catalyst molecule, due to the self-assembly in aqueous solution, to create multivalent nanofibers driven by both the hydrophobic interaction and the hydrogen bonding interaction between two His-Phe dipeptide heads, to form a binding domain (Figure 1b). It was found that Phe, His, and −SH are indispensable because the self-assembled nanofiber, formed from a single minimalistic molecule, has high absolute catalytic activity of the hydrolysis reactions of carboxylic ester substrates, k_{cat}/K_M, which has the dimensions of a second-order rate constant,[35] widely used to make a comparison among different catalytic systems.

RESULTS AND DISCUSSION

A series of minimalistic dipeptide molecules containing a terminal −SH group linked by alkyl chains of varying lengths via an amide bond (marked as HS-C$_{n+1}$-His-Phe, n = 4, 7, 11, 15, and 17; n + 1 represents the carbon atom number of the alkyl chain), and the control compounds were synthesized, as shown in Schemes S1−S11. Three carboxylic ester substrates (DNPB, p-NPB, and DNPA) were also synthesized (Schemes S12−S15), and one substrate is commercially available p-NPA used in this work, considering the effect of hydrophobicity (DNPB vs DNPA, and p-NPB vs p-NPA), and the electron-withdrawing capability (DNPB vs p-NPB, and DNPA vs p-NPA). We first used HS-C$_{16}$-His-Phe to check the catalytic reaction for the substrate p-NPA, p-nitrophenylacetate, one of the commonly used model substrates. As shown in Figure S1 (black line), when HS-C$_{16}$-His-Phe and p-NPA were mixed in 10 mM HEPES buffer solution of pH 7.4 containing 10% MeCN which was used to ensure full dissolution of the thiol and substrate, the absorbance at 400 nm, originating from liberated p-nitrophenol anion due to its charge transfer effect, significantly increased with increasing the reaction time. Together with the hardly observed background reaction of p-NPA in the absence of HS-C$_{16}$-His-Phe, the result supports

https://doi.org/10.1021/acsomega.2c06972
ACS Omega 2023, 8, 2491−2500

that HS-C_{16}-His-Phe can significantly accelerate the hydrolysis reaction of *p*-NPA. In fact, such hydrolysis reactions can also occur in other three substrates in the presence of HS-C_{16}-His-Phe.

The catalytic hydrolysis reaction was directly probed by conducting high-resolution mass spectrometry (HRMS) experiments in the *p*-NPA solution in the presence of HS-C_{16}-His-Phe. The measured HRMS *m*/*z* signal of 138.0190 (Figure S2d) can well match with the theoretically calculated value of the *p*-nitrophenol anion of 138.0197 ($[M-H]^-$), supportive of the breakdown of the carbonyl ester bond. The relationship of the initial rate of this catalytic reaction and *p*-NPA concentration is found to follow the Michaelis−Menten equation (Figure 2d), with k_{cat} = 0.019 ± 0.001 s^{-1}, K_M = 1.8 ± 0.05 mM, and k_{cat}/K_M = 10.6 ± 0.2 $M^{-1}\cdot s^{-1}$. k_{cat} and k_{cat}/K_M are generally used to indicate the intrinsic and absolute catalytic efficiencies of a catalyst, respectively.[35] The effect of the hydrophobicity and electron-withdrawing capability of the substrates on the hydrolysis reaction was subsequently checked. In addition to *p*-NPA, for other tested substrates, all dependences of the initial rates on the substrate concentrations for HS-C_{16}-His-Phe are well consistent with the Michaelis−Menten equation (Figure 2a−c), too. These fittings afford a comparison of their k_{cat}, K_M, and k_{cat}/K_M values, summarized in Table S1. Clearly, the *n*-butyryl group tethered in substrates DNPB and *p*-NPB has a more hydrophobic contribution to the overall molecular structures than that of the acetyl group linked in substrates DNPA and *p*-NPA, respectively. These observations indicate that the higher binding affinity between HS-C_{16}-His-Phe and the substrate can be obtained when the more hydrophobic substrates are used since the reciprocal of the Michaelis−Menten constant K_M is related to the binding affinity between the enzyme and the substrate.[36] Compared to the k_{uncat} values of the tested substrates (the background reactions, summarized in Table S2), all k_{cat} values increase ∼3 orders of magnitude, also supportive of the catalytic nature of this dipeptide. The HRMS experiments of the solutions of other three substrates in the presence of HS-C_{16}-His-Phe also further confirm the occurrence of the hydrolysis reactions to liberate nitrophenol anions (Figure S2a−c). The k_{cat}/K_M values of *p*-NPB and DNPB are higher than those of *p*-NPA and DNPA, respectively. These results again support that increasing the hydrophobicity of the substrates is more helpful to improve their binding affinity toward HS-C_{16}-His-Phe, resulting in the improvement of the absolute catalytic efficiency (k_{cat}/K_M). This observation is consistent with comparing the change of their $1/K_{TS}$ values in which $K_{TS} = k_{uncat}/(k_{cat}/K_M)$ (Table S3), used to indicate the catalytic proficiency, too.[37] Furthermore, when we evaluate the effect of electron-withdrawing capability of the substrates by comparing K_M or k_{cat}/K_M values of the substrates DNPB vs *p*-NPB and DNPA vs *p*-NPA, experimental results further support that the higher binding affinity can result in higher absolute catalytic efficiency. Introducing an additional $-NO_2$ substituent on substrates not only can increase its ability to enter the hydrophobic microenvironment,[38] but also can show an important contribution to weaken the strength of ester bonds, considering that the pK_a of 2,4-dinitrophenol of 2.1 is lower than that of *p*-nitrophenol of 6.2 measured under the experimental conditions in this work, due to the electron-withdrawing effect of the $-NO_2$ substituent (Figure S3).

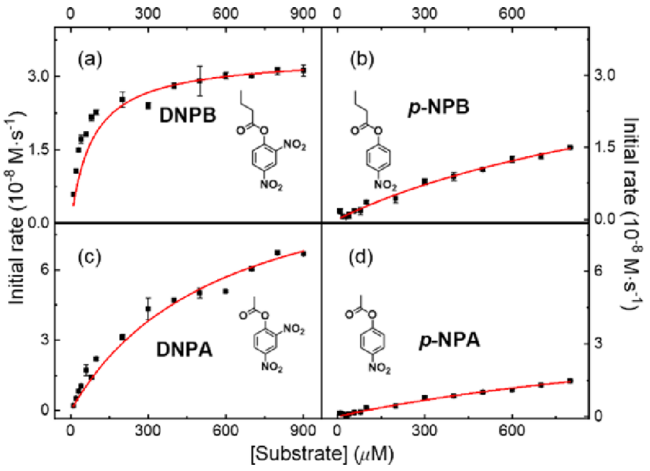

Figure 2. Initial rate as a function of the concentration of substrates DNPB (a), *p*-NPB (b), DNPA (c), and *p*-NPA (d), respectively, in the presence of HS-C_{16}-His-Phe, fitted by the Michaelis−Menten equation (red lines). Experimental conditions (a−d): [HS-C_{16}-His-Phe] = 2.5 μM; 10 mM HEPES buffer solution of pH 7.4 containing 10% MeCN; temperature was set as 37 °C. All error bars in this work were obtained through measuring three parallel experiments.

Next, we changed the length of the hydrophobic alkyl chain of the dipeptide molecules to check their catalytic activity toward DNPB as the substrate. First, to determine their apparent critical aggregation concentration (CAC), a fluorescent probe (Nile Red, NR) method was used. We observed that the CAC values decrease with increasing the *n* number (from 30 to 2.5 μM) until the CAC value nearly levels off at *n* = 15 and 17, indicating that increasing hydrophobicity can lead to the decrease of CAC (Figure S4). When the concentration of HS-C_{n+1}-His-Phe was set as corresponding CAC, the relationships between the initial rate and DNPB concentration were well fitted by the Michaelis−Menten equation (Figure S5). We observed that K_M values of HS-C_{n+1}-His-Phe (*n* = 4, 7, 11, 15, and 17) roughly decrease with increasing the *n* number (Figure 3 and Table S4). This means that the binding affinity between DNPB and the dipeptide molecule increases with the increase of hydrophobicity of the dipeptides. Although the k_{cat} values of these catalysts show a small difference in the intrinsic catalytic activity, a study of the relationship between k_{cat}/K_M values and *n* number shows an increase tendency in particular in the cases of *n* = 11, 15, and 17 (Figure 3). The high k_{cat}/K_M value was observed in HS-C_{16}-His-Phe and HS-C_{18}-His-Phe cases, 358.4 ± 18.6 and 518.3 ± 3.7 $M^{-1}\cdot s^{-1}$, respectively. The nearly reverse relationship between K_M and k_{cat}/K_M values (Figure 3) indicates that the alkyl chain length dependent-absolute catalytic efficiency should be mainly driven by their K_M values. Furthermore, we compared the k_{cat}/K_M values of both the assembly state and nonassembly state (maybe oligomers) in the cases of HS-C_{18}-His-Phe and HS-C_{16}-His-Phe, respectively. It was found that k_{cat}/K_M values of HS-C_{16}-His-Phe in its non-assembly state and assembly state are 118.4 ± 4.0 and 358.4 ± 18.6 $M^{-1}\cdot s^{-1}$, respectively. Also, k_{cat}/K_M values of HS-C_{18}-His-Phe in its nonassembly state and assembly state are 322.0 ± 3.7 and 518.3 ± 3.7 $M^{-1}\cdot s^{-1}$, respectively (Figure S6 and Table S5). This result supports that the self-assembly of the catalysts should play an important role in the catalysis reaction. For evaluating the stability of the self-assembled catalysts with different lengths of alkyl chains toward the catalysis reaction, we conducted the catalytic

https://doi.org/10.1021/acsomega.2c06972
ACS Omega 2023, 8, 2491−2500

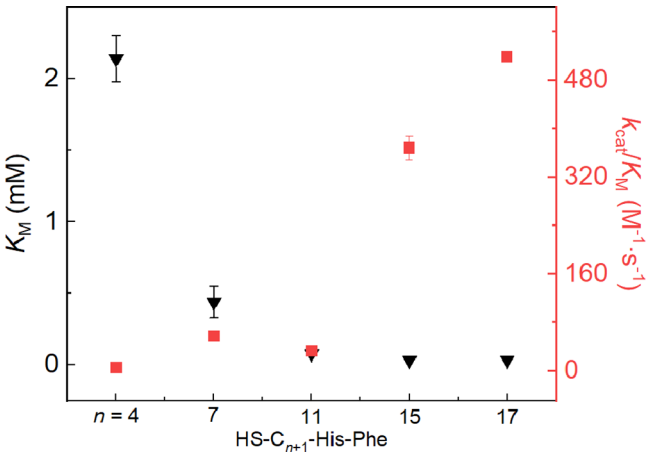

Figure 3. Relationship of K_M or k_{cat}/K_M of DNPB catalyzed by HS-C_{n+1}-His-Phe and n number. Black downright triangles represent K_M, and red squares represent k_{cat}/K_M. Experimental conditions: HS-C_{n+1}-His-Phe are 30 μM (n = 4), 20 μM (n = 7), 10 μM (n = 11), 2.5 μM (n = 15), and 2.3 μM (n = 17); 10 mM HEPES buffer solution of pH 7.4 containing 10% MeCN; temperature was set as 37 °C. All error bars in this work were obtained through measuring three parallel experiments.

hydrolysis reaction experiments of the same self-assembled catalysts under different duration times toward DNPB (transferring the identical volumes of the catalyst stock solution into HEPES buffer solution to obtain different duration times and then conducting the catalysis reaction). In all HS-C_{n+1}-His-Phe cases, it was found that the k_{cat}/K_M values show slight changes with changing duration times, from 0 to 36 h (Figure S7 and Table S6). The slight change in k_{cat}/K_M may originate from a small change in the morphology and/or size of self-assembled nanofibers with different duration times.

We used SEM experiments to probe the morphologies of HS-C_{n+1}-His-Phe aggregates in aqueous solutions. HS-C_5-His-Phe only shows an irregular and lumpy morphology (Figure 4a), quite different from that of other HS-C_{n+1}-His-Phe (n = 7, 11, 15, and 17) which can self-assemble to form observable nanofibers (Figure 4b−e). The morphologic difference between HS-C_5-His-Phe and other tested HS-C_{n+1}-His-Phe (n = 7, 11, 15, and 17) is also supported by the results of TEM experiments (Figure S8). A phosphotungstic acid negatively staining method was further used to afford clearer TEM images in HS-C_{18}-His-Phe, HS-C_{16}-His-Phe, and HS-C_{12}-His-Phe samples. Unambiguous nanofibrous structures could be observed (Figure 4g−i). The diameters calculated from ImageJ software are 10.3 ± 0.9 nm for HS-C_{12}-His-Phe, 21.6 ± 1.3 nm for HS-C_{16}-His-Phe, and 21.9 ± 2.0 nm for HS-C_{18}-His-Phe, respectively, on the basis of their negatively stained TEM images. The fiber-like aggregates were further verified by using laser scanning confocal microscope experiments, in which the catalyst aqueous solutions were directly used to observe the images, rather than the dried sample, affording a more convincing support for the formation of nanofibers in aqueous solution (Figure S9). A single nucleation event followed by uniform growth in the fast and slow directions, in analogy to living polymerization, should be considered as a possible mechanism of self-assembled nanofiber formation.[39,40] Besides microscope experiments, ^{1}H NMR spectra of 50 μM HS-C_{n+1}-His-Phe (5% CD_3OD + 95% H_2O) were recorded on an 850 MHz NMR instrument to afford a supporting for the aggregation, too. It is found that the H chemical shift from alkyl chains gradually disappears in the fine signals and broadens with increasing the number of n from 7 to 17 under identical concentration (Figure 4f). This result, together with the results of SEM and TEM, supports that the aggregation of HS-C_{n+1}-His-Phe bearing a long alkyl chain in the aqueous solution to create nanofibrous morphology is strengthened, compared with that containing a short alkyl chain.[41]

Furthermore, theoretical calculation was further conducted to probe the molecular aggregation behaviors of HS-C_{n+1}-His-Phe. The optimal structures of dimers in the aqueous solution, calculated at the B3LYP method and the 6-31g(d) basis set by using the Gaussian 09 program suite,[42] reveal that the energies of the cases of HS-C_{16}-His-Phe and HS-C_{18}-His-Phe are significantly lower than cases of n = 5, 8, and 12 (Figure 4j−n). This energy difference supports that HS-C_{16}-His-Phe and HS-C_{18}-His-Phe more easily form a dimer and even further self-assemble with extended conformations to achieve ordered chain arrangements in aqueous solution, compared to those with a relatively short chain.

Considering the use of dipeptide as a catalyst, the pH-dependent-absolute catalytic activity was studied in HS-C_{16}-His-Phe case. Two pK_a values occur in this curve profile. The first pK_a of 4.2 originates from the terminal carboxylate of Phe, and the second pK_a of 6.4 can be assigned to the imidazole moiety of His (Figure 5). This observation is similar to the previously reported work in which the dipeptide was clustered on the surface of Au nanoparticles.[31] The decrease of pK_a of imidazole in this work, compared with alone imidazole (6.8), supported its aggregate state, likely originating from the contribution of local hydrophobicity of the aggregate.[43] However, pK_a of the −SH group was hardly observed in this case, likely because (i) when pH was enhanced to close to pK_a of imidazole (6.4), −SH groups from the catalysts have started to transform into RS^- due to the involvement of imidazole to the deprotonation of R-SH,[44] considering its pK_a of 8.3,[45] and with increasing pH to 7.4 almost 99% −SH groups have been transformed into RS^-. This means that the inflection region ascribed to that of imidazole has contained the contribution of RS^-. (ii) The actual nucleophile may be the thiol (a much poorer nucleophile than the thiolate, though) and the proton is transferred once the nucleophilic attack has occurred. The involvement of imidazole to the deprotonation of R-SH has also been reported by Baker.[46] We are also curious to know what will happen to the catalytic activity for the ester hydrolysis if the His, Phe, and −SH moieties of the dipeptide molecule are alternately removed. Therefore, we synthesized the control compounds, HS-C_{16}-His, HS-C_{16}-Phe, C_{16}-His-Phe, and HO-C_{16}-His-Phe, by removing Phe, His, and −SH, and changing the −SH group into the −OH group in HS-C_{16}-His-Phe, respectively (Figure 6a). These compounds were used as the catalyst, respectively, to the hydrolysis reaction of DNPB. Considering that these catalysts likely self-assemble in aqueous solutions, CAC values were also determined by using a fluorescent probe (NR) method (Figure S10). When the catalyst concentration was set as the corresponding CAC, DNPB was used to conduct Michaelis−Menten equation experiments (Figure S11). These catalytic parameters are listed in Table S7. Very intriguingly, seen from Figure 6b, the k_{cat}/K_M values of HS-C_{16}-His and HS-C_{16}-Phe are found to drop to 50.7 ± 1.8 and 5.4 ± 1. 8 $M^{-1}\cdot s^{-1}$, respectively, compared with that of HS-C_{16}-His-Phe (358.4 ± 18.6 $M^{-1}\cdot s^{-1}$). These

https://doi.org/10.1021/acsomega.2c06972
ACS Omega 2023, 8, 2491−2500

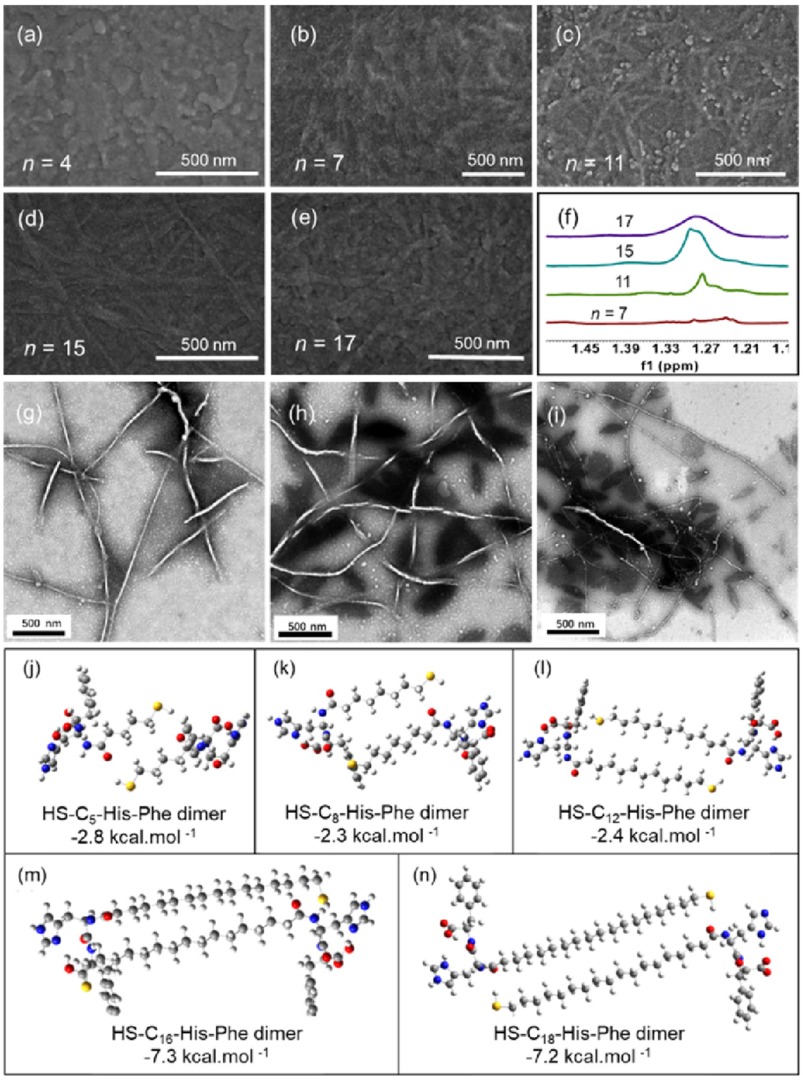

Figure 4. Scanning electron microscopy (SEM) images of the HS-C_{n+1}-His-Phe (n = 4, (a); n = 7, (b); n = 11, (c); n = 15, (d); n = 17, (e)), partial proton nuclear magnetic resonance (^{1}H NMR) of HS-C_{n+1}-His-Phe (5% CD_3OD + 95% H_2O) obtained on an 850 MHz NMR instrument (f), and negatively stained transmission electron microscopy (TEM) images of the HS-C_{n+1}-His-Phe (n = 17, (g); n = 15, (h); n = 11, (i)). Optimal structures of the HS-C_{n+1}-His-Phe dimers (j–n), In (j–n), the yellow, blue, and red big balls represent S, N, and O atoms, respectively, and the small and big gray balls represent H and C atoms, respectively.

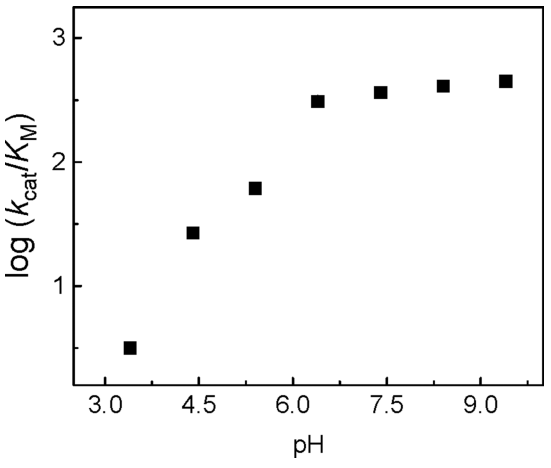

Figure 5. pH-dependent log(k_{cat}/K_M) of HS-C_{16}-His-Phe.

decreases of 1–2 orders of magnitude fully demonstrate the importance of the His-Phe dipeptide head for this ester hydrolysis reaction. In fact, the imidazole moiety of the His acting as a general base role was found to be an important active-site in many natural esterases such as α-ChS,[47] as mentioned in the Introduction. The k_{cat}/K_M values of C_{16}-His-Phe without a terminal −SH group and of HO-C_{16}-His-Phe containing a terminal −OH group are 1.3 ± 0.7 and 53.9 ± 1.8 $M^{-1}\cdot s^{-1}$, respectively, also lower 1–2 orders of magnitude than that of HS-C_{16}-His-Phe, supportive of the importance of the −SH group. Moreover, this is reasonable since the nucleophilic ability of the −SH group is higher than that of −OH[48] and introducing a terminal −OH group significantly weakens its hydrophobicity, supported by the difference of their CAC values. Furthermore, when the long hexadecanoyl chain is changed into the short acetyl group to create Ac-His-Phe (Figure 6a), its k_{cat}/K_M value of 1.2 ± 0.1 $M^{-1}\cdot s^{-1}$, nearly close to that of C_{16}-His-Phe, is indicative of the importance of introducing −SH, again. In fact, the oxidation experiments of H_2O_2 can substantially support that the contribution to the catalysis reaction is −SH group rather than the assumed

https://doi.org/10.1021/acsomega.2c06972
ACS Omega 2023, 8, 2491−2500

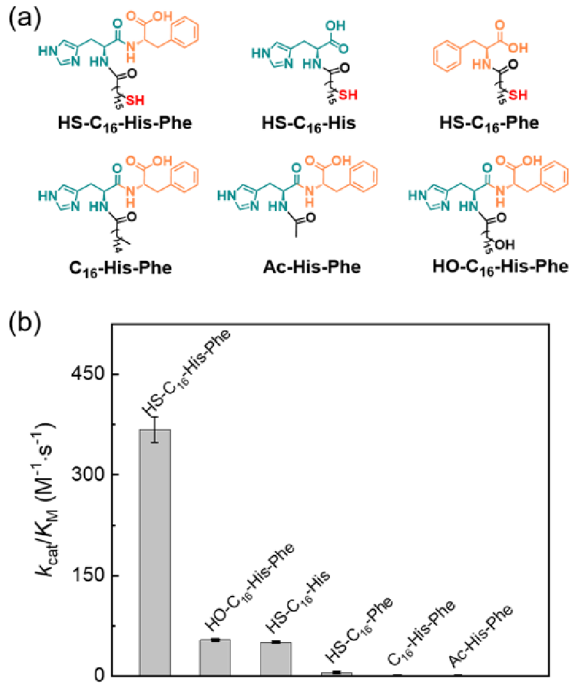

Figure 6. Molecular structures of HS-C_{16}-His-Phe and the control catalysts (a). Comparisons of k_{cat}/K_M for the hydrolysis reaction of substrate DNPB catalyzed by HS-C_{16}-His-Phe and its control compounds (b). Experimental conditions: [HS-C_{16}-His-Phe] = 2.5 μM, [HO-C_{16}-His-Phe] = 18 μM, [HS-C_{16}-His] = 9 μM, [HS-C_{16}-Phe] = 9 μM, [C_{16}-His-Phe] = 160 μM, [Ac-His-Phe] = 100 μM, respectively; 10 mM HEPES buffer solution of pH 7.4 containing 10% MeCN; temperature = 37 °C.

disulfide compound in the aqueous solution (see the Supporting Information, Figure S12).

All taken together, we can primarily propose that the O atom of the carbonylate group of Phe is hydrogen bonded by the H atom of H−N in the imidazole moiety to increase the pK_a of imidazole leading to a stronger general base, similar to the interaction between His and Asp moieties in α-ChS since it possesses a popular Ser-His-Asp triad.[34] The N atom of the imidazole ring can deprotonate the terminal −SH group from adjacent another catalyst molecule via the intermolecular aggregation, or from the same catalyst molecule via intramolecular folding, to form a strong nucleophile to attack the carboxylic ester bond of the substrate, thus likely leading to a suitable binding domain composed of a hydrogen bonding acceptor ($-CO_2^-$ of Phe), base (−imidazole of His) and nucleophile (−SH). The −SH group used as a nucleophile in enzymatic mimicking the hydrolysis reaction of carboxylic ester has also been demonstrated.[45,47] For example, Woolfson[44] used a heptameric peptide CC-Hept-Cys-His-Glu assembly containing the −SH group to mimic enzyme behavior toward the hydrolysis reaction of *p*-NPA. This catalysis hydrolysis reaction showed a two-step process, the formation (fast kinetic burst) and hydrolysis (slow turnover kinetics) of the thioester intermediate, respectively. Therefore, enlightened by their research, we also conducted the experiments of reaction time-dependent release of the 2,4-DNP anion, indicating a distinct two-state kinetic profile in HS-C_{16}-His-Phe case of our work (Figure S13a). This result is similar to the observation reported by Woolfson,[44] involving a covalently bound acyl intermediate. Furthermore, the *y*-intercept of the second state curve of this profile is matched with the added catalyst concentration (Figure S13a, black line). This indicates that the intermediate is bound on the dipeptide. We further tried to afford the rate constants of the two steps in our work by using an empirical function containing a single exponential and a linear component:[44] $y = a[1 - e^{-b \cdot t}] + c[1 - e^{-d \cdot t}] + L \cdot t$ (in which y is the concentration of catalyst, a and c are the observed burst amplitude, b and d are the observed single exponential burst rate constant, and L is the observed linear rate constant), fitted by SigmaPlot software (Figure S14), and the fitting curve corresponding to two steps is shown in Figure S13a (red line). The rate constant of burst was calculated to be 0.0062 s^{-1}, 1 order of magnitude higher than of turn-over phase (62 times), 0.0001 s^{-1} (Table S8). The HRMS experiments of the reaction solution revealed a measured m/z signal peak at 671.3741, well matched with the theoretically calculated m/z value of the assumed thioester intermediate, 641.3742 ($[M-H]^-$), monitored in both reaction times of 5 and 20 min, as shown in Figure 7a,b. Importantly, the abundance of MS signal peaks at 671.3741 of the acylated intermediate in the reaction time of 20 min (Figure 7b) is lower 20 times than that in the reaction time of 5 min (Figure 7a). Besides this, the abundance of MS signal peaks of HS-C_{16}-His-Phe (m/z found at 571.3325 or 571.3320), consistent with its theoretically calculated m/z value, 571.3324 ($[M-H]^-$), increased by ∼1 order of magnitude with extending the reaction time from 10 min (Figure 7c) to 30 min (Figure 7d), substantially confirming that the relatively rapid release of HS-C_{16}-His-Phe occurred in the turn-over phase. These results can afford evidence for the thiol group being a nucleophilic role to the hydrolysis reaction of carboxylic ester. Indeed, HS-C_{16}-His-Phe can show a robust catalysis with more than 34 turnovers (5 μM catalyst vs 200 μM DNPB) for extending the reaction time to 5 h (Figure S14b). Although we made considerable efforts to try to validate the catalytic mechanism, the assumed triad, we have to acknowledge that other possible pathways maybe exist in our system, considering that actual assembly structures have not been fully understood so far.

To further compare this catalytic efficiency (k_{cat}/K_M) with that of natural enzymes, α-ChS was used to catalyze the hydrolysis reaction of DNPB under identical experimental conditions (Figure S15). The k_{cat}/K_M of α-ChS was measured to be 397.1 ± 1.1 $M^{-1}\cdot s^{-1}$, far smaller than that of HS-C_{18}-His-Phe (k_{cat}/K_M of 518.3 ± 3.7 $M^{-1}\cdot s^{-1}$), and close to that of HS-C_{16}-His-Phe (358.4 ± 18.6 $M^{-1}\cdot s^{-1}$). Furthermore, k_{cat} values for both HS-C_{16}-His-Phe (0.01 s^{-1}) and HS-C_{18}-His-Phe (0.02 s^{-1}) are higher than that of α-ChS (0.009 s^{-1}). We should point out that although this synthetic multivalent catalyst system is comparable to natural α-ChS at intrinsic and absolute catalytic efficiencies, at least, this does mean our system is completely superior to α-ChS, considering that DNPB is a synthesized substrate rather a natural substrate. In fact, we are pleased to observe that, when the cases of using the same substrate are compared, the k_{cat}/K_M values (n = 15 and 17) in this work are 1 order magnitude higher than that of monolayer-protected Au NPs (∼10 $M^{-1}\cdot s^{-1}$) via using similar dipeptide molecules containing a terminal −SH group to cluster on the surface.[31] Besides k_{cat}/K_M, k_{cat} values in our present work (0.01 s^{-1} for n = 15 and 0.02 s^{-1} for n = 17) are also two orders of magnitude higher than that in this reported work (1.5×10^{-4} s^{-1}).[31] We consider that the low catalytic efficiency in their work is likely attributed to the sacrifice of the −SH group used as the nucleophile due to the formation of Au−SR bonds, although the multivalent nature occurs. The

https://doi.org/10.1021/acsomega.2c06972
ACS Omega 2023, 8, 2491−2500

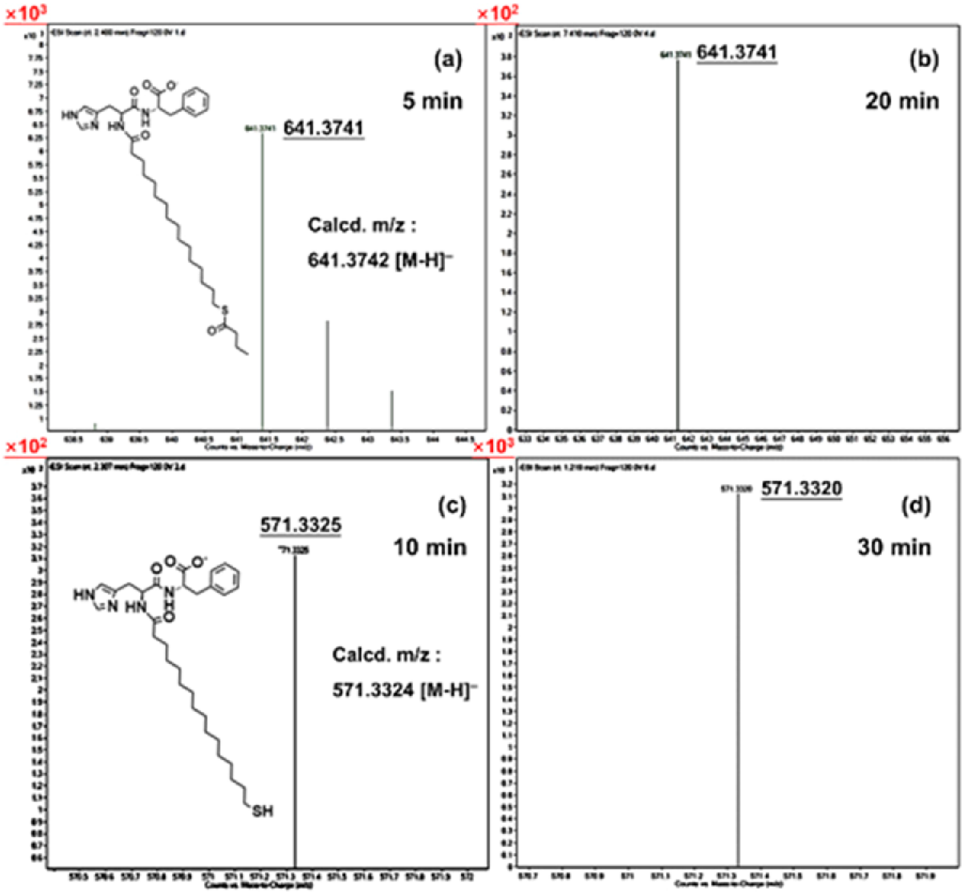

Figure 7. HRMS results for probing the thioester intermediate in the hydrolysis reaction of 20 μM DNPB catalyzed by 2.5 μM HS-C_{16}-His-Phe for 5 min (a) and 20 min (b), and HRMS results for probing released HS-C_{16}-His-Phe in the hydrolysis reaction of 20 μM DNPB catalyzed by 2.5 μM HS-C_{16}-His-Phe for 10 min (c) and 30 min (d).

comparison of k_{cat}/K_M values of other examples and this work, using *p*-NPA or other representative carboxylic esters as the substrate, was summarized in Table 1. Although the exact comparison of these studies is hardly achieved due to the differences of the substrates and experimental conditions, our work looked outstanding in the absolute catalytic efficiency.

Table 1. k_{cat}/K_M Values for the Hydrolysis Reactions of Carboxylic Esters in Previously Reported Cases and This Work Used Peptides as the Basic Catalytic Units

catalyst	pH	substrate	k_{cat}/K_M ($M^{-1}\cdot s^{-1}$)
dipeptide-coated Au[31]	7.0	DNPB	~10
Au-PEP[24]	7.0	DNPB	~100
H1/Au MPC 1[18]	7.0	Cbz-Phe-ONP	473
Hg-Zn-TRIL9CL23H[3]	7.5	*p*-NPA	1.38
Ac-IHIHIQI-$CONH_2$[17]	8.0	*p*-NPA	3.7
CC-Hept-Cys-His-Glu[44]	7.0	*p*-NPA	22
HS-C_{18}-His-Phe (this work)	7.4	*p*-NPA	12.4
HS-C_{18}-His-Phe (this work)	7.4	DNPB	518.3

CONCLUSIONS

In conclusion, a His-Phe dipeptide head and a terminal −SH group were linked by a hydrophobic alkyl chain with varying lengths to create one class of minimalistic dipeptide molecules, HS-C_{n+1}-His-Phe (n = 4, 7, 11, 15, and 17) to create multivalent nanofiber structures via self-assembly in aqueous solution, that can catalyze the hydrolysis reactions of carboxylic esters. The catalytic activity generally increases with increasing n number and can reach 358.4 ± 18.6 $M^{-1}\cdot s^{-1}$ (n = 15) and 518.3 ± 3.7 $M^{-1}\cdot s^{-1}$ (n = 17) for the k_{cat}/K_M value. In addition to the outstanding catalytic efficiency, this minimalistic dipeptide system can show high substrate specificity when four substrates were used to compare their K_M and k_{cat}/K_M values. The His, Phe, and −SH moieties and long hydrophobic alkyl chains were found to be indispensable for this catalytic hydrolysis reaction with such exciting efficiencies, challengeable to natural α-ChS at reaction rate (k_{cat} and k_{cat}/K_M), at least, strictly speaking, toward the substrate DNPB. The system presented in this work allows for several intriguing possibilities, including the possibility of changing the length of hydrophobic alkyl chain to tune the catalytic activity when other catalytic units are used, and the possibility of adding more examples to bridge the gap between structural complexity and minimalist, by changing the catalytic units. Furthermore, if less activated carboxylic esters[49,50] catalyzed by such a system are considered, the *p*-nitro-phenol moiety, functioned as the UV−vis absorption signal, can be replaced by a fluorescent molecule containing a −OH group to create a non-fluorescent and less activated carboxylic ester, probed by fluorescence spectra, in future work.

EXPERIMENTAL SECTION

Materials. Catalysts, control catalysts, and substrates including DNPA, DNPB, and *p*-NPB mentioned by this

https://doi.org/10.1021/acsomega.2c06972
ACS Omega 2023, 8, 2491−2500

work were synthesized. *p*-NPA, NR, α-ChS, and other chemicals and solvents were commercially purchased. The ultrapure water was obtained from a Milli-Q system.

Synthesis and Characterization of Catalysts and Substrates. For the detailed synthesis procedures, refer to the Supporting Information (Schemes S1−S15), and ^{1}HNMR, ^{13}C NMR, and MS characterization studies are shown in Figures S15−S104.

Measuring pK_a Values of *p*-Nitrophenol and 2,4-Dinitrophenol Anions. The UV−Vis absorption spectra of *p*-nitrophenol and 2,4-dinitrophenol with 50 μM concentrations in buffer solutions containing 10% MeCN with varying pH values (pH = 3.4, 4.4, 5.4, 6.4, and 7.4 for 2,4-dinitrophenol; pH = 5.4, 6.4, 7.4, 8.4, and 9.4 for *p*-nitrophenol) were measured to afford absorbance at 400 nm (*p*-nitrophenol anion) and 410 nm (2,4-dinitrophenol anion). The pK_a values of *p*-nitrophenol anion and 2,4-dinitrophenol anion were obtained by fitting the equation in the Supporting Information.

Michaelis−Menten Equation Kinetics. HS-C_{n+1}-His-Phe used as the catalysts to the hydrolysis reactions of carboxylic ester substrates was probed by measuring the change of the reaction time dependent-absorbance at 400 or 410 nm wavelength, respectively: a certain volume of the HS-C_{n+1}-His-Phe stock solution and a series of volumes of substrate stock solution (from 0 to 600 μL) were mixed in 5 mL test tubes, respectively. The total volume was kept at 3 mL by adding a certain volume of 10 mM HEPES buffer solution of pH 7.4 containing 10% MeCN, leading to HS-C_{n+1}-His-Phe final concentration that was at the corresponding CAC concentrations and the final concentration of substrate was from 0 to 1000 μM. Absorbance at 410 nm (for DNPB and DNPA) and 400 nm (for *p*-NPB and *p*-NPA) of the reaction solution was monitored on a recorded by a UV-2600 spectrometer (Shimadzu, Japan) in which the scanning time was extended to 5 min at 37 °C.

The initial rate was calculated from the reaction time dependent-absorbance of 2,4-dinitrophenol anion (for DNPB and DNPA) at 410 nm or *p*-nitrophenol (for *p*-NPB and *p*-NPA) anion at 400 nm evolving curves. The reaction product *p*-nitrophenol anion or 2,4-dinitrophenol anion concentration could be determined, according to the molar absorption coefficient (ε) of 2,4-dinitrophenol anion (for DNPB and DNPA) and *p*-nitrophenol anion (for *p*-NPB and *p*-NPA) which was found to be 11645.7 and 9742.7 L·mol^{-1}·cm^{-1}, respectively.

Electrospray Ionization-Mass Spectrometry (ESI-MS) Experiments for Probing the Hydrolysis Reactions. HS-C_{16}-His-Phe concentration was set as 3 μM, the substrate concentration was set as 20 μM, and the temperature was kept at 37 °C for 20 min. The reaction solution was then injected into the ESI-MS system for obtaining desirable ESI-MS spectra.

Probing CAC by a Fluorescent Probe NR Method. Ten microliters of 0.5 mM NR stock solution and 2 mL of 10 mM HEPES buffer solution of pH 7.4 containing 10% MeCN were added into a 5 mL test tube to obtain a series of test tubes containing 2.5 μM NR. After that, different amounts of catalyst were added into each test tube, respectively, and these test tubes were kept for 30 min at room temperature to record their fluorescence spectra. The excitation wavelength was used as 564 nm. The experiments are carried out on an F-7000 fluorescence spectrometer (Hitachi, Japan).

Determining pH-Dependent log(k_{cat}/K_M) Profile. Buffer solutions used (10 mM, containing 10% MeCN) are citric acid/sodium citrate (pH = 3.4), acetic acid/sodium acetate (pH = 4.4 and 5.4), MES (pH = 6.4), HEPES (pH = 7.4), Tris−HCl (pH = 8.0), and CHES (pH = 9.4). Experimental conditions: [HS-C_{16}-His-Phe] = 2.5 μM, DNPB was chosen to conduct Michaelis−Menten kinetics experiments, and the test temperature was set as 37 °C.

850 MHz ^{1}H NMR Spectra of HS-C_{n+1}-His-Phe. HS-C_{n+1}-His-Phe was dissolved in 5% CD_3OD−95% H_2O mixing solvent to afford 50 μM at concentration, and the chemical shift signal in the range of 1.20−1.34 ppm was collected by an 850 MHz/AVANCE III system (Bruker, Switzerland).

Morphology Characterization. *SEM.* The HS-C_{n+1}-His-Phe samples were dissolved in water/acetonitrile mixed solvent (the volume ratio of water to acetonitrile is 9/1) to afford the concentration slightly higher than their corresponding CAC values, respectively, and 10 μL of the prepared solution was taken on the silicon wafer. After the samples were dried at room temperature, another 10 μL of the prepared solutions were taken again on the same sample spot on the silicon wafer to repeat the dry procedure to obtain SEM samples. Then, the morphologies of the samples were observed on a field emission scanning electron microscope (FESEM, S-4800, Hitachi, Japan).

TEM. For TEM samples without a staining procedure, 3 μL of the above HS-C_{n+1}-His-Phe sample solution in SEM experiments was dropped on ultrathin carbon-supported copper mesh, respectively. Then, the samples were dried at room temperature to obtain TEM samples. For negatively stained TEM samples, 3 μL of the above HS-C_{n+1}-His-Phe sample solution was dropped on ultrathin carbon-supported copper mesh, respectively. Next, the filter paper was used to suck the droplets away from the edge to retain a thin liquid film. Then, the copper meshes covered with the sample were carefully buckled on the phosphotungstic acid solution (1%) for 1 min and subsequently were carefully taken out and dried at room temperature to conduct TEM experiments. Then, the morphologies were observed through a transmission electron microscope (TEM, H-7650, Hitachi, Japan).

Laser Scanning Confocal Microscope. One milliliter of the above HS-C_{n+1}-His-Phe sample solution in SEM experiments and 5 μL of 0.5 mM NR solution were mixed, and then 5 μL the mixed solution was dropped on a glass slide. The dropped glass slide was carefully covered by another glass slide, and the sample was placed into the uploading sample position of a laser scanning confocal microscope, and images were obtained from a Leica TCS SP8 instrument (Leica, Germany) equipped with a 552 nm laser for obtaining images.

Theoretical Calculations. The electronic structures, optimized geometries, and frequency properties of the monomers and dimers of HS-C_5-His-Phe, HS-C_8-His-Phe, HS-C_{12}-His-Phe, HS-C_{16}-His-Phe, and HS-C_{18}-His-Phe were calculated at the B3LYP method and the 6-31g(d) basis set using the Gaussian 09 program suite.[42] The harmonic vibrational frequencies were computed to verify that each geometry was a true minimum and was found to have no negative frequencies for the most stable structures. The solvent effect was considered using the SMD continuum solvent model, which takes into account the full solute electron density in calculating the solvation energy.

https://doi.org/10.1021/acsomega.2c06972
ACS Omega 2023, 8, 2491−2500

■ ASSOCIATED CONTENT

Supporting Information

The Supporting Information is available free of charge at https://pubs.acs.org/doi/10.1021/acsomega.2c06972.

The routes of synthesis (Schemes S1−S15), the experimental procedures of synthesis, and the characterization of catalysts and substrates, the experimental procedures of measuring basic catalytic parameters, and theoretical calculations, and supporting experimental results (Figures S1−S104 and Tables S1−S8) (PDF)

■ AUTHOR INFORMATION

Corresponding Author

Jiang-Shan Shen − *Xiamen Key Laboratory of Optoelectronic Materials and Advanced Manufacturing, College of Materials Science and Engineering, Huaqiao University, Xiamen 361021, China*; orcid.org/0000-0002-3584-3564; Email: jsshen@hqu.edu.cn

Authors

Ning Liu − *Xiamen Key Laboratory of Optoelectronic Materials and Advanced Manufacturing, College of Materials Science and Engineering, Huaqiao University, Xiamen 361021, China*

Shuai-Bing Li − *Xiamen Key Laboratory of Optoelectronic Materials and Advanced Manufacturing, College of Materials Science and Engineering, Huaqiao University, Xiamen 361021, China*

Yan-Zhen Zheng − *College of Ocean Food and Biological Engineering, Jimei University, Xiamen 361021, China*

Su-Ying Xu − *State Key Laboratory of Chemical Resource Engineering, Beijing Key Laboratory of Environmentally Harmful Chemical Analysis, Beijing University of Chemical Technology, Beijing 100029, China*

Complete contact information is available at: https://pubs.acs.org/10.1021/acsomega.2c06972

Notes

The authors declare no competing financial interest.

■ ACKNOWLEDGMENTS

This work was supported by the Fujian Provincial Department of Science and Technology (No. 2020Y0038), the Xiamen Municipal Bureau of Science and Technology (No. 3502Z20193029), and the Instrumental Analysis Center of Huaqiao University. We also thank Dr. Xiao-Sheng Yan at Xiamen University for his help to ^{1}H NMR experiments on an 850 MHz instrument and thank Prof. Yun-Bao Jiang at Xiamen University and four reviewers for their enlightening comments on this work.

■ REFERENCES

(1) Garcia-Viloca, M.; Gao, J.; Karplus, M.; Truhlar, D. G. How Enzymes Work: Analysis by Modern Rate Theory and Computer Simulations. *Science* **2004**, *303*, 186−195.

(2) Deniz, A. A. Enzymes Can Adapt to Cold by Wiggling Regions Far from Their Active Site. *Nature* **2018**, *558*, 195−196.

(3) Zastrow, L. M.; Peacock, A. F. A.; Stuckey, J. A.; Pecoraro, V. L. Hydrolytic Catalysis and Structural Stabilization in a Designed Metalloprotein. *Nat. Chem.* **2012**, *4*, 118−123.

(4) Diez-Castellnou, M.; Mancin, F.; Scrimin, P. Efficient Phosphodiester Cleaving Nanozymes Resulting from Multivalency and Local Medium Polarity Control. *J. Am. Chem. Soc.* **2014**, *136*, 1158−1161.

(5) Cravatt, B. F.; Giang, D. K.; Mayfield, S. P.; Boger, D. L.; Lerner, R. A.; Gilula, N. B. Molecular Characterization of an Enzyme that Degrades Neuromodulatory Fatty-Acid Amides. *Nature* **1996**, *384*, 83−87.

(6) Bryan, P. N. Prodomains and Protein Folding Catalysis. *Chem. Rev.* **2002**, *102*, 4805−4816.

(7) Sharma, A.; Hartwig, J. F. Metal-Catalysed Azidation of Tertiary C-H Bonds Suitable for Late-Stage Functionalization. *Nature* **2015**, *517*, 600−604.

(8) Wangikar, P. P.; Rich, J. O.; Clark, D. S.; Dordick, J. S. Probing Enzymic Transition State Hydrophobicities. *Biochemistry* **1995**, *34*, 12302−12310.

(9) Nakamura, H.; Xue, Y. L.; Miyakawa, T.; Hou, F.; Qin, H. M.; Fukui, K.; Shi, X.; Ito, E.; Ito, S.; Park, S. H.; Miyauchi, Y.; Asano, A.; Totsuka, N.; Ueda, T.; Tanokura, M.; Asami, T. Molecular Mechanism of Strigolactone Perception by DWARF14. *Nat. Commun.* **2013**, *4*, 2613.

(10) Zhou, G. W.; Guo, J. C.; Huang, W.; Fletterick, R. J.; Scanlan, T. S. Crystal Structure of a Catalytic Antibody with a Serine Protease Active Site. *Science* **1994**, *265*, 1059−1064.

(11) Buller, A. R.; Townsend, C. A. Intrinsic Evolutionary Constraints on Protease Structure, Enzyme Acylation, and the Identity of the Catalytic Triad. *Proc. Natl. Acad. Sci. U. S. A.* **2013**, *110*, E653−E661.

(12) Garrido-González, J. J.; Aparicio, M. M. I.; Garcia, M. M.; Simon, L.; Sanz, F.; Moran, J. R.; de Arriba, A. L. F. An Enzyme Model Which Mimics Chymotrypsin and N-Terminal Hydrolases. *ACS Catal.* **2020**, *10*, 11162−11170.

(13) Nothling, M. D.; Xiao, Z. Y.; Hill, N. S.; Blyth, M. T.; Bhaskaran, A.; Sani, M. A.; Espinosa-Gomez, A.; Ngov, K.; White, J.; Buscher, T.; Separovic, F.; O'Mara, M. L.; Coote, M. L.; Connal, L. A. A Multifunctional Surfactant Catalyst Inspired by Hydrolases. *Sci. Adv.* **2020**, *6*, No. eaaz0404.

(14) Elias, M.; Wieczorek, G.; Rosenne, S.; Tawfik, D. S. The Universality of Enzymatic Rate-Temperature Dependency. *Trends Biochem. Sci.* **2014**, *39*, 1−7.

(15) Bommarius, A. S.; Paye, M. F. Stabilizing Biocatalysts. *Chem. Soc. Rev.* **2013**, *42*, 6534−6565.

(16) Nothling, M. D.; Ganesan, A.; Condic-Jurkic, K.; Pressly, E.; Davalos, A.; Gotrik, M. R.; Xiao, Z. Y.; Khoshdel, E.; Hawker, C. J.; O'Mara, M. L.; Coote, M. L.; Connal, L. A. Simple Design of an Enzyme-Inspired Supported Catalyst Based on a Catalytic Triad. *Chem* **2017**, *2*, 732−745.

(17) Rufo, C. M.; Moroz, Y. S.; Moroz, O. V.; Stohr, J.; Smith, T. A.; Hu, X. Z.; DeGrado, W. F.; Korendovych, I. V. Short Peptides Self-Assemble to Produce Catalytic Amyloids. *Nat. Chem.* **2014**, *6*, 303−309.

(18) Zaramella, D.; Scrimin, P.; Prins, L. J. Self-Assembly of a Catalytic Multivalent Peptide-Nanoparticle Complex. *J. Am. Chem. Soc.* **2012**, *134*, 8396−8399.

(19) Gruber, B.; Kataev, E.; Aschenbrenner, J.; Stadlbauer, S.; Konig, B. Vesicles and Micelles from Amphiphilic Zinc(II)-Cyclen Complexes as Highly Potent Promoters of Hydrolytic DNA Cleavage. *J. Am. Chem. Soc.* **2011**, *133*, 20704−20707.

(20) Maiti, S.; Fortunati, I.; Ferrante, C.; Scrimin, P.; Prins, L. J. Dissipative Self-Assembly of Vesicular Nanoreactors. *Nat. Chem.* **2016**, *8*, 725−731.

(21) Zaupa, G.; Scrimin, P.; Prins, L. J. Origin of the Dendritic Effect in Multivalent Enzyme-Like Catalysts. *J. Am. Chem. Soc.* **2008**, *130*, 5699−5709.

(22) Delort, E.; Darbre, T.; Reymond, J. L. A Strong Positive Dendritic Effect in a Peptide Dendrimer-Catalyzed Ester Hydrolysis Reaction. *J. Am. Chem. Soc.* **2004**, *126*, 15642−15643.

(23) Manea, F.; Houillon, F. B.; Pasquato, L.; Scrimin, P. Nanozymes: Gold-Nanoparticle-Based Transphosphorylation Catalysts. *Angew. Chem., Int. Ed.* **2004**, *43*, 6165−6169.

(24) Pengo, P.; Baltzer, L.; Pasquato, L.; Scrimin, P. Substrate Modulation of the Activity of an Artificial Nanoesterase Made of Peptide-Functionalized Gold Nanoparticles. *Angew. Chem., Int. Ed.* **2007**, *46*, 400−404.
(25) Mikolajczak, D. J.; Berger, A. A.; Koksch, B. Catalytically Active Peptide-Gold Nanoparticle Conjugates: Prospecting for Artificial Enzymes. *Angew. Chem., Int. Ed.* **2020**, *59*, 8776−8785.
(26) Solomon, L. A.; Kronenberg, J. B.; Fry, H. C. Control of Heme Coordination and Catalytic Activity by Conformational Changes in Peptide-Amphiphile Assemblies. *J. Am. Chem. Soc.* **2017**, *139*, 8497−8507.
(27) Dolan, M. A.; Basa, P. N.; Zozulia, O.; Lengyel, Z.; Lebl, R.; Kohn, E. M.; Bhattacharya, S.; Korendovych, I. V. Catalytic Nanoassemblies Formed by Short Peptides Promote Highly Enantioselective Transfer Hydrogenation. *ACS Nano* **2019**, *13*, 9292−9297.
(28) Singh, N.; Kumar, M.; Miravet, J. F.; Ulijn, R. V.; Escuder, B. Peptide-Based Molecular Hydrogels as Supramolecular Protein Mimics. *Chem. − Eur. J.* **2017**, *23*, 981−993.
(29) Guler, M. O.; Stupp, S. I. A Self-Assembled Nanofiber Catalyst for Ester Hydrolysis. *J. Am. Chem. Soc.* **2007**, *129*, 12082−12083.
(30) Singh, N.; Tena-Solsona, M.; Miravet, J. F.; Escuder, B. Towards Supramolecular Catalysis with Small Self-Assembled Peptides. *Isr. J. Chem.* **2015**, *55*, 711−723.
(31) Pengo, P.; Polizzi, S.; Pasquato, L.; Scrimin, P. Carboxylate-Imidazole Cooperativity in Dipeptide-Functionalized Gold Nanoparticles with Esterase-Like Activity. *J. Am. Chem. Soc.* **2005**, *127*, 1616−1617.
(32) Cao, Y. J.; Yao, M. X.; Prins, L. J.; Ji, R. X.; Liu, N.; Sun, X. Y.; Jiang, Y. B.; Shen, J. S. Self-Assembled Multivalent Ag-SR Coordination Polymers with Phosphatase-Like Activity. *Chem. − Eur. J.* **2021**, *27*, 7646−7650.
(33) Kleinsmann, A. J.; Nachtsheim, B. J. A Minimalistic Hydrolase Based on Co-Assembled Cyclic Dipeptides. *Org. Biomol. Chem.* **2020**, *18*, 102−107.
(34) Wang, M. F.; Lv, Y. Q.; Liu, X. J.; Qi, W.; Su, R. X.; He, Z. M. Enhancing the Activity of Peptide-Based Artificial Hydrolase with Catalytic Ser/His/Asp Triad and Molecular Imprinting. *ACS Appl. Mater. Interfaces* **2016**, *8*, 14133−14141.
(35) Gabrielli, L.; Prins, L. J.; Rastrelli, F.; Mancin, F.; Scrimin, P. Hydrolytic Nanozymes. *Eur. J. Org. Chem.* **2020**, *2020*, 5044−5055.
(36) Callender, R.; Dyer, R. B. The Dynamical Nature of Enzymatic Catalysis. *Acc. Chem. Res.* **2015**, *48*, 407−413.
(37) Studer, S.; Hansen, D. A.; Pianowski, Z. L.; Mittl, P. R. E.; Debon, A.; Guffy, S. L.; Der, B. S.; Kuhlman, B.; Hilvert, D. Evolution of a Highly Active and Enantiospecific Metalloenzyme from Short Peptides. *Science* **2018**, *362*, 1285−1288.
(38) Zheng, W. R.; Xu, J. L.; Huang, T.; Yang, Q.; Chen, Z. C. Hydrogen Bonding Interaction between Ureas or Thioureas and Nitro-Compounds. *Res. Chem. Intermed.* **2011**, *37*, 31−45.
(39) Cui, H. G.; Muraoka, T.; Cheetham, A. G.; Stupp, S. I. Self-Assembly of Giant Peptide Nanobelts. *Nano Lett.* **2009**, *9*, 945−951.
(40) Hendricks, M. P.; Sato, K.; Palmer, L. C.; Stupp, S. I. Supramolecular Assembly of Peptide Amphiphiles. *Acc. Chem. Res.* **2017**, *50*, 2440−2448.
(41) Palchowdhury, S.; Bhargava, B. L. Effect of Cation Asymmetry on the Aggregation in Aqueous 1-Alkyl, 3-Decylimidazolium Bromide Solutions: Molecular Dynamics Studies. *J. Phys. Chem. B* **2014**, *118*, 6241−6249.
(42) Frisch, M. J.; Trucks, G. W.; Schlegel, H. B.; Scuseria, G. E.; Robb, M. A.; Cheeseman, J. R.; Scalmani, G.; Barone, V.; Mennucci, B.; Petersson, G. A.; Nakatsuji, H.; Caricato, M.; Li, X.; Hratchian, H. P.; Izmaylov, A. F.; Bloino, J.; Zheng, G.; Sonnenberg, J. L.; Hada, M. M.; Ehara, K. T.; Fukuda, R.; Hasegawa, J.; Ishida, M.; Nakajima, T.; Honda, Y.; Kitao, O.; Nakai, H.; Vreven, T.; Montgomery, J. A.; Peralta, Jr., J. E.; Ogliaro, F.; Bearpark, M.; Heyd, J. J.; Brothers, E. K.; Kudin, N.; Staroverov, V. N.; Kobayashi, R.; Normand, J.; Raghavachari, K.; Rendell, A.; Burant, J. C.; Iyengar, S. S.; Tomasi, J.; Cossi, M.; Rega, N.; Millam, N. J.; Klene, M.; Knox, J. E.; Cross, J. B.; Bakken, V.; Adamo, C.; Jaramillo, J.; Gomperts, R.; Stratmann, R. E.; Yazyev, O.; Austin, A. J.; Cammi, R.; Pomelli, C.; Ochterski, J. W.; Martin, R. L.; Morokuma, K.; Zakrzewski, V. G.; VothGA, S. P.; Dannenberg, J. J.; Dapprich, S.; Daniels, A. D.; Farkas, Ö.; Foresman, J. B.; Ortiz, J. V.; Cioslowski, J.; Fox, D. J. *Gaussian 09*; Gaussian, Inc., 2009.
(43) Chadha, G.; Zhao, Y. Histidine-Functionalized Water-Soluble Nanoparticles for Biomimetic Nucleophilic/General-Base Catalysis under Acidic Conditions. *Org. Biomol. Chem.* **2013**, *11*, 6849−6855.
(44) Burton, A. J.; Thomson, A. R.; Dawson, W. M.; Brady, R. L.; Woolfson, D. N. Installing Hydrolytic Activity into a Completely *De Novo* Protein Framework. *Nat. Chem.* **2016**, *8*, 837−844.
(45) Donald, V.; Judith, G.V. *Biochemistry*, 4th edition; John Wiley & Sons, 2010.
(46) Richter, F.; Blomberg, R.; Kuzin, A.; Tong, L.; Hilvert, D.; Baker, D. Computational Design of Catalytic Dyads and Oxyanion Holes for Ester Hydrolysis. *J. Am. Chem. Soc.* **2012**, *134*, 16197−16206.
(47) Nothling, M. D.; Xiao, Z. Y.; Bhaskaran, A.; Blyth, M. T.; Bennet, C. W.; Coote, M. L.; Connal, L. A. Synthetic Catalysts Inspired by Hydrolytic Enzymes. *ACS Catal.* **2019**, *9*, 168−187.
(48) McGrath, N. A.; Raines, R. T. Chemoselectivity in Chemical Biology: Acyl Transfer Reactions with Sulfur and Selenium. *Acc. Chem. Res.* **2011**, *44*, 752−761.
(49) Lee, Y. J.; Devaraj, N. K. Lipase mimetic cyclodextrins. *Chem. Sci.* **2021**, *12*, 1090−1094.
(50) Arifuzzaman, M. D.; Bose, I.; Bahrami, F.; Zhao, Y. Imprinted Polymeric Nanoparticles as Artificial Enzymes for Ester Hydrolysis at Room Temperature and pH 7. *Chem. Catal.* **2022**, *2*, 2049−2065.

https://doi.org/10.1021/acsomega.2c06972
ACS Omega 2023, 8, 2491−2500